MULTI-OBJECTIVE PARAMETRIC OPTIMISATION OF MASKED STEREOLITHOGRAPHY ADDITIVE MANUFACTURING USING THE RESPONSE SURFACE METHOD

J.A. Dicks[1*], M.I. Hoosain[1] & O. Mbele[1]

ARTICLE INFO

Article details
Presented at the 25th Annual International Conference of the Rapid Product Development Association of South Africa (RAPDASA) Institute for Industrial Engineering, held from 28 October to 31 October 2024 in Gqeberha, South Africa

Available online 13 Dec 2023

Contact details
* Corresponding author
james.dicks@uct.ac.za

Author affiliations
1 Centre for Materials Engineering, Department of Mechanical Engineering, University of Cape Town, Cape Town, South Africa

ORCID® identifiers
J.A. Dicks
https://orcid.org/0000-0001-7529-3678

M.I. Hoosain
http://orcid.org/0009-0005-1897-1272

O. Mbele
http://orcid.org/0000-0001-6928-795X

DOI
http://dx.doi.org//10.7166/35-4-3147

ABSTRACT

Masked stereolithography is an effective and economical additive manufacturing technology that is suitable to fabricate objects for engineering applications. As such, parametric optimisation to attain good mechanical properties is of value in order to realise its full potential. A multi-objective optimisation of the printing parameters of masked stereolithography 3D printing for mechanical properties was performed using central composite design for response surface method analysis. The developed response surfaces were used to perform numerical optimisation to establish appropriate printing parameters, which were validated against experimental results and compared with bulk polymer specimen mechanical properties. Here, an optimised layer cure time of 3.8 s, a layer height of 50 µm, and a post-curing time of 13.5 min resulted in mechanical properties closely predicted by the model and near to bulk polymer specimen properties. Last, the optimisation results were related to a Jacobs working curve, which established that layer cure times beyond that determined by the Jacobs working curve were favoured.

OPSOMMING

Gemaskerde stereolitografie is 'n effektiewe en ekonomiese toevoegingsmiddelvervaardigingstegnologie wat geskik is om voorwerpe vir ingenieurstoepassings te vervaardig. Daarom is parametriese optimering om goeie meganiese eienskappe te bereik van waarde om die volle potensiaal daarvan te verwesenlik. 'n Multi-objektiewe optimering van die drukparameters van gemaskerde stereolitografie 3D-drukwerk vir meganiese eienskappe is uitgevoer met behulp van sentrale saamgestelde ontwerp vir responsoppervlakmetode-analise. Die ontwikkelde responsoppervlaktes is gebruik om numeriese optimering uit te voer om toepaslike drukparameters daar te stel, wat bekragtig is teen eksperimentele resultate en vergelyk is met meganiese eienskappe van grootmaat polimeermonster. Hier het 'n optimum laaguithardingstyd van 3.8 s, 'n laaghoogte van 50 µm en 'n na-uithardingstyd van 13.5 min gelei tot meganiese eienskappe wat noukeurig deur die model voorspel is en naby aan grootmaat polimeermonster eienskappe. Laastens was die optimeringsresultate verwant aan 'n Jacobs-werkkromme, wat vasgestel het dat laaguithardingstye verder as wat deur die Jacobs-werkkurwe bepaal is, bevoordeel is.

1. INTRODUCTION

The use of vat photopolymerisation additive manufacturing (AM) has become increasingly popular in engineering contexts, and a proliferation in fabrication technologies has occurred in recent years [1-3]. Of these developments, masked stereolithography (mSLA) has presented itself as an economical and effective AM technology [4]. Here, an LCD screen is used to generate a layer pattern by selectively masking a uniform UV array of LEDs, thus facilitating uniform irradiation, high resolutions, and simultaneous entire layer photopolymerisation. However, mSLA 3D printing is based on layer-by-layer fabrication, thus exposing itself to the negative impacts associated with material anisotropy. It is also well established that the printing parameters and post-fabrication treatments affect the mechanical properties [5-7]. The optimisation of the mechanical properties of components manufactured using AM is appreciably important in order to exploit fully its potential in engineering contexts, as these fabrication technologies shift away from rapid prototyping and proof-of-concept applications towards final product fabrication. Several numerical models and parametric optimisation studies have been established for AM, yet there is still a distinct lack of empirical studies about optimising multi-objective mechanical behaviour. Given that a number of 3D printing parameters can influence the polymer's mechanical properties, a design of experiments (DoE) approach (e.g., Taguchi method, Box-Behnken) has established itself as a robust method for parametric optimisation in vat photopolymerisation AM [8-21]. Central composite design (CCD) for response surface method (RSM) analysis is another efficient DoE method for optimisation that has been explored [22-25]. Here, CCD is a fractional factorial design, composed of a cube, a star, and a central point, that can be used for non-linear descriptive models to establish interactions between multiple factors and levels [26, 27]. However, few studies have focused on mechanical behaviour, but have investigated only ultimate tensile strength (UTS) as a mechanical response [24, 28]. While this has laid a firm basis for applying CCD and RSM analysis, it is well known that optimisation for UTS alone may not provide a comprehensive understanding of the mechanical properties of a given polymer. Examining multi-objective responses thus opens the opportunity to provide a more nuanced optimisation for balanced mechanical properties. Furthermore, using CCD for RSM analysis allows for numerical optimisation to be performed in order to ascertain the most suitable 3D printing parameters for optimised mechanical properties. Underlying the principle of mechanical property optimisation is the fundamental competing effect of homogeneous material behaviour versus heterogeneous interlayer effects in layer-by-layer AM technologies. As such, a relationship between the optimisation of printing parameters and the monomer system photopolymerisation reaction was also sought using a Jacobs [29] working curve to understand further the basis of the optimisation of mechanical properties in mSLA 3D printing.

2. MATERIALS AND METHODS

2.1. Materials

eSun PLA-Pro transparent resin (eSun, Taiwan) was purchased from DIYElectronics (South Africa). Propan-2-ol (99%) was purchased from Kimix Chemicals (South Africa). All materials were used as received.

2.2. Design of experiments and analysis

2.2.1. Design of experiments

A face-centred CCD with a star point distance (α) of 1 was used to develop the DoE using Stat-Ease Design-Expert v.23.1.1 software. Within the CCD, three factors with three levels each were chosen on the basis of commonly employed fabrication parameters, as outlined in Table 1.

Table 1: Factors and levels used in the CCD DoE

Factor	Level		
Layer height (µm)	50	75	100
Layer cure time (s)	3	4	5
Post-curing time (min)	0	10	20

Responses were observed for both horizontal and vertical printing orientations. The tensile modulus, ultimate tensile strength, tensile strain at break, flexural modulus, ultimate flexural strength, flexural strain at break, and Charpy impact energy were measured as responses, along with their anisotropy ratios with respect to printing orientation.

2.2.2. Analysis

The responses for the DoE were computed in Stat-Ease Design-Expert v.23.1.1 software. Model process orders were chosen on the basis of the sequential p-value, lack-of-fit p-value, adjusted R^2, and predicted R^2. The analysis of variance (ANOVA) of the model, factors, and factor interactions used a p-value < 0.05 as significant. Insignificant terms in the model were removed using a backwards elimination regression of p-values.

2.3. Experiments

2.3.1. Masked stereolithography additive manufacturing

Additive manufacturing was performed using a mSLA 3D printer (Sonic Mini 4K, Phrozen, Taiwan) installed with a removable magnetic spring steel build platform. A layer height of 50 µm, 75 µm, or 100 µm, a bottom layer cure time of 35 s for the first four layers, and normal layer cure times of 3–6 s were used. A lift distance of 5 mm, a lift speed of 60 mm/min, and a retract speed of 80 mm/min were used between layers. The irradiance of the 3D printer 405 nm LED array was 2.39 mW/cm^2. After 3D printing, the specimens were briefly washed in isopropanol using a washing station (UW-02, Creality, Taiwan) and dried prior to post-curing.

2.3.2. Jacobs working curve

A Jacobs [29] working curve, in accordance with the Beer-Lambert law, was used to establish the relationships between irradiance and depth of cure. An array of 25 blocks (10 x 10 mm^2) was printed with varying incident radiant exposures (E_0) using irradiation times (t_0) between 1 s and 25 s, performed independently in triplicate. This was performed in the 3D printer vat with at least 20 mm depth of resin that had been left to settle for 24 hours to minimise the effect of dissolved oxygen. The excess resin was then carefully poured out of the vat, followed by sequential washing of the polymer array with isopropanol until the voxel grid pattern appeared, indicating that no further uncured resin was present on its surface, and the isopropanol was evaporated. The cure depth (C_d) of the specimens was measured using a digital micrometer (Digimatic MDC-25MX, Mitutoyo, Japan) with a resolution of 1 µm and a maximum permissible error of ±1 µm. C_d was plotted as a function of $ln(E_0)$, and a least-squares linear fit of the plot was used to provide the characteristic penetration depth (D_p) from the slope and critical incident radiant exposure for gelation (E_c) from the x-intercept of the extrapolated plot, according to equation 1.

$$C_d = D_p \, ln\left(\frac{E_0}{E_c}\right) \quad (1)$$

2.3.3. Bulk polymer specimen preparation

Bulk polymer specimens were prepared by pouring the resin into Teflon moulds with geometries according to ASTM D638-22 Type V specimens [30] and ASTM D790-17 specimens [31]. The resins were then irradiated using a 395 nm LED UV lamp with an irradiance of 67 mW.cm^{-2} for 120 s; the samples were then turned over and irradiated for a further 120 s, thus providing a total of 16 J of radiant energy. Five specimens were prepared for mechanical testing.

2.4. Mechanical testing

2.4.1. Tensile testing

The specimens were prepared in accordance with ASTM D638-22 with Type V specimen geometries. Tensile testing was performed on a universal testing machine (Zwick 1484, Zwick-Roell, Germany) equipped with 10 kN loadcell and a crosshead speed of 5 mm/min. Displacement was measured using an integrated video extensometer (LIMESS Messtechnik und Software GmbH, Germany). Young's modulus (E_t), ultimate tensile stress (σ_t), and tensile strain at break (ε_t) were calculated according to ASTM D638-22. The specimen geometries were measured using a Vernier calliper (Mitutoyo, Japan) with a resolution of 20 µm.

2.4.2. Three-point flexural testing

The specimens were prepared in accordance with ASTM D790-17 [31] with sample geometries of 60.0 × 12.0 × 3.2 mm^3. Three-point flexural tests were performed on a universal testing machine (Instron 3365, Norwood, MA, USA) equipped with 1 kN loadcell, using a span length of 45.00 mm and a crosshead speed of 1mm/min. Flexural modulus (E_f), flexural strength (σ_f), and flexural strain at break (ε_f) were calculated according to ASTM D790-17. The specimen geometries were measured using a Vernier calliper (Mitutoyo, Japan) with a resolution of 20 µm.

2.4.3. Charpy v-notch impact testing

The specimens were prepared in accordance with ASTM D6110-18 [32]. Testing was performed on a pendulum impact tester (Zwick GmbH & Co., Germany) with a 2 J pendulum and release angle of 160°. The specimen geometries were measured using a Vernier calliper (Mitutoyo, Japan) with a resolution of 20 µm.

3. RESULTS

3.1. DoE and ANOVA of models

The use of CCD to generate the design of experiments resulted in the experimental matrix outlined in Table A1. Once the experimental response results had been entered into the DoE matrix, model fitting was performed for each of the responses. All the responses fitted a quadric order process, with the exception of the ultimate flexural strength anisotropy ratio, which fitted a two-factor influence order process model. The models were then analysed using ANOVA to ascertain statistically significant (p-value <0.05) factor and interaction coefficients. The ANOVA results (Tables A2-A19) of the sum of squares, degrees of freedom, mean squares, F-value, and p-values indicated that all quadratic models were significant with insignificant lack-of-fit, indicating the models' validity. However, not all the first- and second-order coefficients in the models were significant. Of particular note, only the post-cure time primary coefficient was significant for the tensile strength and tensile strength anisotropy ratio in the horizontal printing direction; the layer cure time primary coefficient was not significant for the tensile modulus anisotropy ratio; and the layer height primary coefficient was not significant for tensile strain in the horizontal printing direction. Insignificant coefficients were removed from the models by a backwards elimination regression of p-values >0.05, and thus they did not influence the models for further response surface optimisations. The R^2, adjusted R^2, and predicted R^2 values (Table A20) accounted for discrepancies between the experimental data and the models, such that values near to 1 indicated a good correlation. The R^2 and adjusted R^2 values were generally high, with the exception of several of the anisotropy ratio responses. The predicted R^2 value, which provides an estimate of the models' ability to predict new responses from the response surface, should generally be close (<0.2 difference) to the adjusted R^2 value. This was generally found to be the case, with the exception of the anisotropy ratio responses. The anisotropy ratio responses displayed low or negative predicted R^2 values that were >0.2 from the adjusted R^2 values, suggesting overfitting, and thus rendering these models without appreciable predictive benefit. Where predicted R^2 values were less than 0.5, the models were deemed inappropriate for use in numerical optimisation and thus were not included. Last, the adequate precision ratios of the included models were >4, indicating adequate model discrimination from signal-to-noise ratios. The response model equations (Tables A21 and A22) for both the actual and the coded equations could thus be obtained and used to generate response surface plots and be used in numerical optimisations.

3.2. Response surface plots

Response surface plots of the tensile modulus for the interaction between layer cure time and post-cure time could be generated as significant interactions in both the horizontal (Fig. 1a) and the vertical (Fig. 1b) printing directions. While there was no interaction between layer height and layer cure time in the horizontal printing direction, the interaction between these factors was significant in the vertical printing direction (Fig. 1c). A general increase in tensile modulus was observed with increasing post-curing time, while higher a tensile modulus was observed for smaller layer heights and intermediate layer cure times.

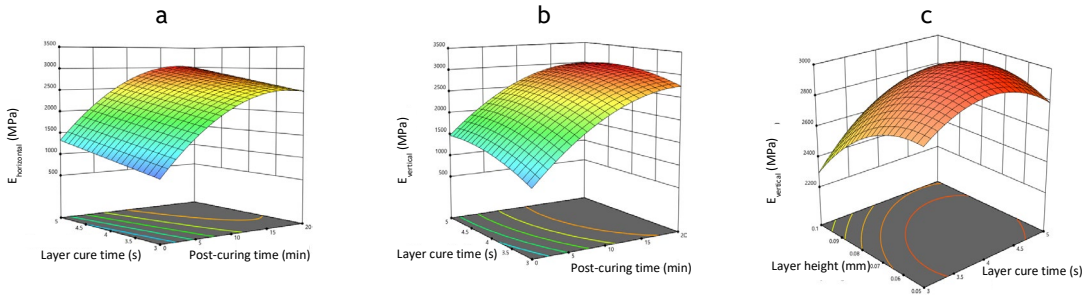

Figure 1: Response surface plot of tensile modulus in the a) horizontal printing direction as a function of layer cure time and post-cure time, b) vertical printing direction as a function of layer cure time and post-cure time, and c) vertical printing direction as a function of layer height and layer cure time.

For the tensile strength, the response surface plots for the interaction between layer cure time and post-cure time were significant in both the horizontal (Fig. 2a) and the vertical (Fig. 2b) printing directions. Furthermore, the interaction between layer cure time and layer height in the vertical printing direction was significant (Fig. 2c). A general increase in tensile strength was observed with increasing post-curing time, while higher tensile strength was observed for smaller layer heights and longer layer cure times.

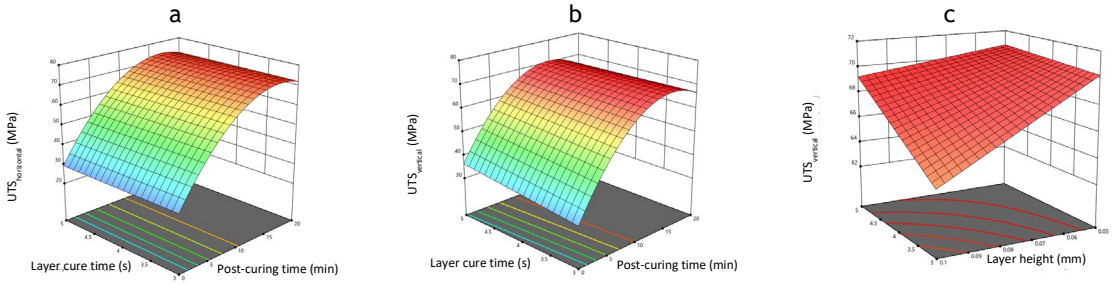

Figure 2: Response surface plots of ultimate tensile strength in the a) horizontal printing direction as a function of layer cure time and post-cure time, b) vertical printing direction as a function of layer cure time and post-cure time, and c) vertical printing direction as a function of layer height and layer cure time.

The interaction between the layer cure time and the post-cure time was significant for the tensile strain in both printing directions (Figs 3a and b). Initially, a decrease in tensile strain was observed with increasing post-curing time. However, a local minimum in tensile strain was observed in both the horizontal and the vertical printing direction, such that further post-curing resulted in a slight increase in the tensile strain. Furthermore, a local maximum in the response surface was apparent for an intermediate layer cure time of around 4 s throughout all post-curing times in the vertical printing direction.

a b

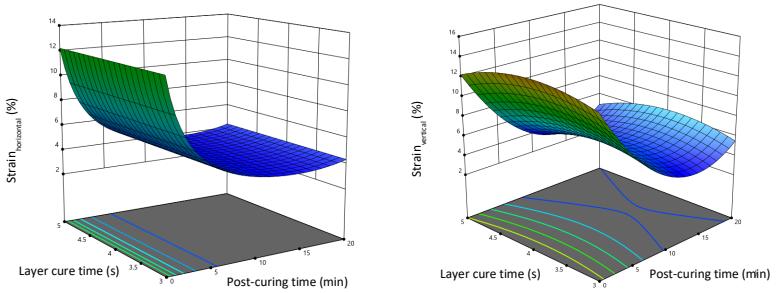

Figure 3: Response surface plot of tensile strain a) horizontal printing direction as a function of layer cure time and post-cure time, and b) vertical printing direction as a function of layer cure time and post-cure time.

For the flexural modulus, the interactions between both layer height and layer cure time with post-curing time were significant in both the horizontal (Figs 4a and b) and the vertical (Figs 4c and d) printing directions. An increase in the flexural modulus was observed with longer post-curing times in both printing directions, although a local maximum at times less than 20 min was observed. In both directions, a greater flexural modulus was also observed for longer layer cure times and smaller layer heights at low post-curing times, which became less apparent at longer post-curing times.

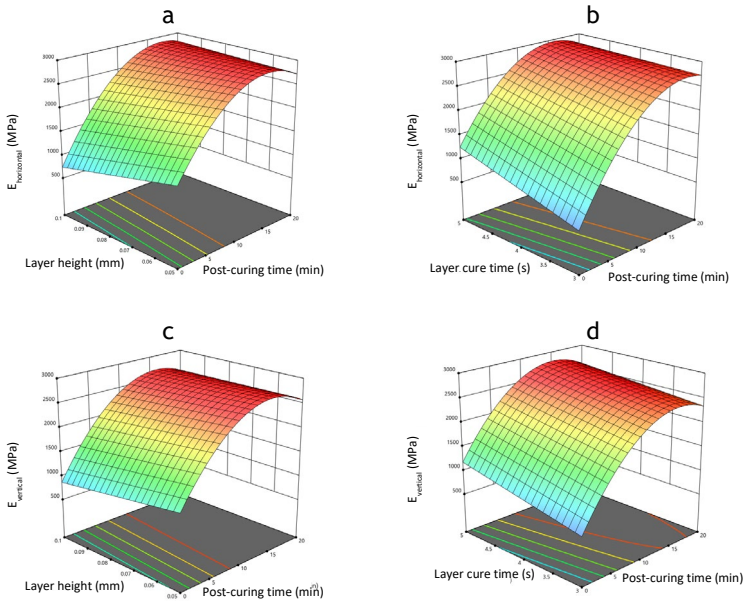

Figure 4. Response surface plot of flexural modulus in a) the horizontal printing direction as a function of layer height and post-cure time, b) the horizontal printing direction as a function of layer cure time and post-cure time, c) the vertical printing direction as a function of layer cure time and post-cure time, and d) the vertical printing direction as a function of layer height and post-cure time.

For the flexural strength, the interaction between the layer cure time and the post-cure time was significant in both printing directions (Figs 5a and c), while the interaction between the layer height and the post-cure time was only significant in the horizontal print direction (Fig. 5b). An increase in the flexural strength was observed with longer post-curing times, although a local maximum at times less than 20 min was observed in both printing directions. In the vertical printing direction, a higher modulus was also observed for longer layer cure times and smaller layer heights at low post-curing times, which became less pronounced at longer post-curing times.

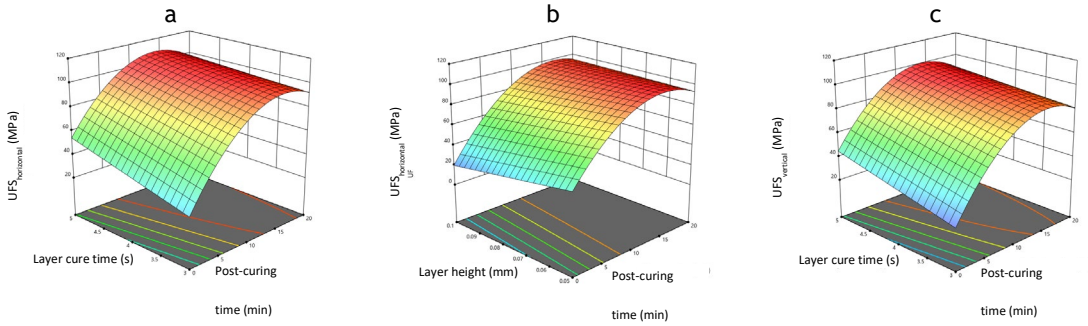

Figure 5: Response surface plot of flexural strength in a) the horizontal printing direction as a function of layer cure time and post-cure time, b) the horizontal printing direction as a function of layer height and post-cure time, and c) the vertical printing direction as a function of layer cure time and post-cure time.

All the factors displayed significant interactions for the flexural strain in the horizontal printing direction (Figs 6a-c), while only the interaction between layer height and layer cure time (Fig. 6d) and layer height and post-cure time (Fig. 6e) was significant in the vertical printing direction. A decrease in flexural strain with increasing post-curing time was observed, while complex interactions between layer height and layer cure time were apparent.

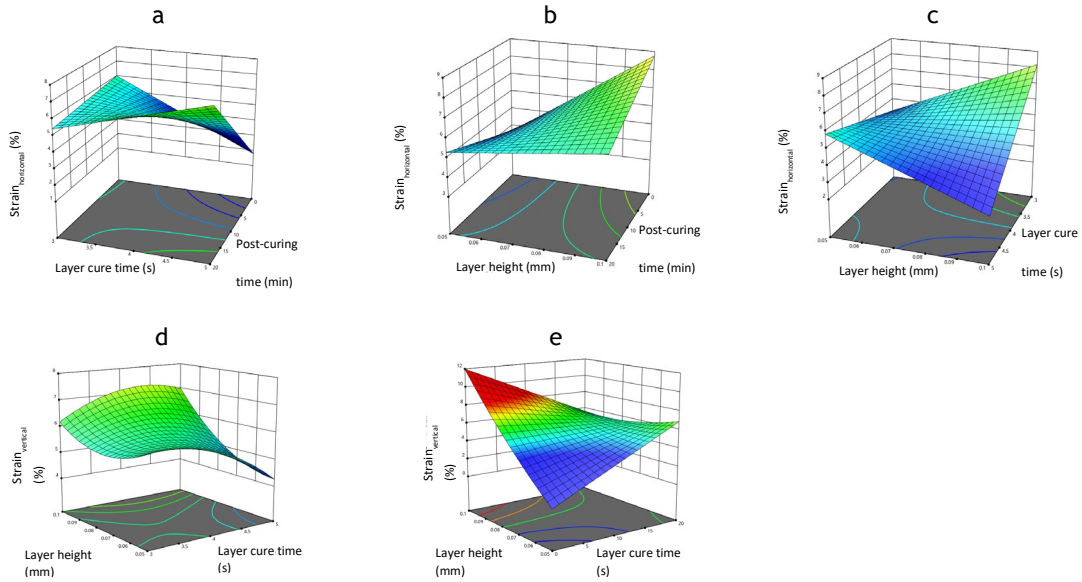

Figure 6: Response surface plot of flexural strain in a) the horizontal printing direction as a function of layer cure time and post-cure time, b) the horizontal printing direction as a function of layer height and post-cure time, c) the horizontal printing direction as a function of layer height and layer cure time, d) the vertical printing direction as a function of layer height and layer cure time, and e) the vertical printing direction as a function of layer height and post-cure time.

3.3. Numerical optimisation

Using the previously generated response surface plots, numerical optimisation resulted in printing parameters of a 50 µm layer height, a layer cure time of 3.82 s, and a post-curing time of 13.5 min, with the predicted mechanical properties outlined in Table 2.

Although models with low predicted R^2 values were not used in the numerical optimisation, their predicted response values were still ascertained to investigate their predictive efficacy. Using the numerical models' optimised printing parameters, experimental testing was performed to ascertain discrepancies between the models' predicted responses and the experimental responses (Table 2). The predicted and the experimental responses were predominantly in good agreement with one another, with errors of <5% for most responses. However, both the tensile strain and the flexural strain in the vertical printing direction deviated considerably between the predicted and the experimental responses. Likewise, the Charpy impact properties deviated between the predicted and the experimental responses, which was unsurprising, given the low predicted R^2 values that were obtained for these models.

Table 2: Predicted and experimental responses for optimised 3D printing parameters

Response	Print direction	Predicted	Experimental	Error
Tensile modulus (MPa)	Horizontal	2910	2967±97	-1.92%
	Vertical	2939	2904±102	1.21%
	Anisotropy	1.03	1.02	0.42%
Tensile strength (MPa)	Horizontal	72.4	71.9±1.1	0.77%
	Vertical	70.6	69.4±1.2	1.88%
	Anisotropy	1.03	1.04	-0.79%
Tensile strain (%)	Horizontal	4.49	4.29±0.24	4.54%
	Vertical	5.57	5.02±0.16	9.84%
	Anisotropy	0.87	0.85	2.00%
Flexural modulus (MPa)	Horizontal	2915	2902±84	0.46%
	Vertical	2713	2681±56	1.21%
	Anisotropy	1.02	1.08	-5.49%
Flexural strength (MPa)	Horizontal	106.1	102.1±0.6	3.80%
	Vertical	100.5	97.8±0.7	2.72%
	Anisotropy	1.09	1.04	3.80%
Flexural strain (%)	Horizontal	6.55	6.49±1.22	0.96%
	Vertical	4.94	4.54±0.80	8.00%
	Anisotropy	1.14	1.43	-20.46%
Charpy impact ($J.cm^{-2}$)	Horizontal	3684	3035±208	21.40%
	Vertical	2586	2864±94	-9.69%

3.4. Bulk polymer specimen properties

To support an understanding of the influence of the 3D printing process on the mechanical properties, the mechanical properties of bulk polymer specimens were investigated and compared with the mechanical properties of the 3D printed specimens that had been previously obtained using optimised printing parameters, as outlined in Table 4. The bulk polymer specimens for Charpy impact testing were not prepared, given the poor predictive capabilities of these models.

Table 3: Mechanical properties of bulk polymers and comparison with optimised 3D printed specimens

		Difference between bulk and 3D printed polymers	
Mechanical property	**Bulk polymer**	**Horizontal print direction**	**Vertical print direction**
Tensile modulus (MPa)	2982 ± 23	0.5%	3%
Tensile strength (MPa)	70.7 ± 0.64	2%	2%
Tensile strain (%)	5.04 ± 0.20	15%	0.5%
Flexural modulus (MPa)	2718 ± 21	7%	1%
Flexural strength (MPa)	98.9 ± 2.67	3%	1%
Flexural strain (%)	6.21 ± 0.40	4%	26%

3.5. Jacobs working curve

The Jacobs working curve, established on the premise of the Beer-Lambert law, provides an indication of the incident UV radiant exposure to achieve a specific cure depth, which can be used to inform layer cure time for a specific layer height in layer-by-layer AM. The Jacobs working curve produced an acceptable linear least-squares fit with an R^2 value of 0.99, indicating the normal behaviour expected of acrylate thermosetting polymers [33-36]. From the plot (Fig. 7), a critical time for gelation (t_c) of 1.82 s and a D_p of 170.57 µm were obtained. An overlay of the experimental layer cure times and layer heights was incorporated to demonstrate the relative position of the printing parameters that were used to develop the models experimentally. From the linear least-squares fit, minimum layer cure times of 2.5 s, 2.8 s, and 3.2 s were found for 50 µm, 75 µm, and 100 µm layer heights respectively. Although a layer cure time of 3 s for the 100 µm layer height fell to the left of the Jacobs working curve, 3D prints could still be successfully obtained. This may have been because these parameters fell within the standard error of the plot, thus implying that sufficient UV exposure was still provided for gelation throughout the layer.

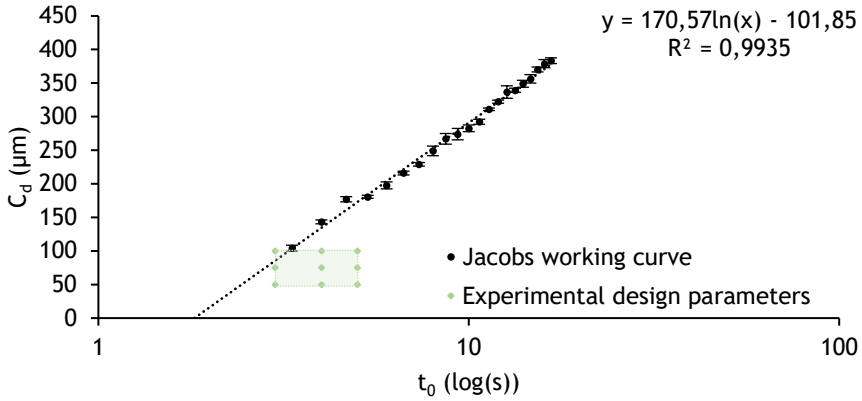

Figure 7: Jacobs working curve and experimental design space

In order to establish a relationship between the layer cure times obtained from the Jacobs working curve and those for optimised mechanical properties, numerical optimisation was performed using fixed layer heights (100 µm, 75 µm, 50 µm) to ascertain the layer cure times for optimised responses (Table 4). It was evident that layer cure times appreciably greater than t0 were obtained for the optimised responses, with 1.2-1.3s cure time differences. These results were plotted alongside the Jacobs working curve (Fig. 8) so that a near linear relationship (R2 > 0.99) could be obtained. Furthermore, all the optimised layer cure times for the three chosen layer heights resulted in a post-curing time of around 13 min.

Table 4: 3D printing parameters

	Layer height (µm)		
	50	75	100
Working curve layer cure time (s)	2.5	2.8	3.2
Optimised layer cure time (s)	3.8	4.1	4.5
Difference (s)	1.3	1.2	1.3
Optimised post-cure time (min)	13.5	13.3	13.1

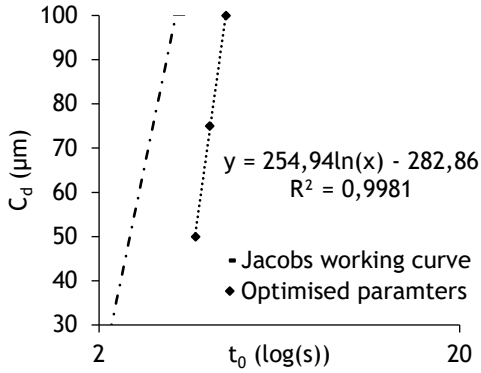

Figure 8: Optimised layer cure times

4. DISCUSSION

4.1. DoE and analysis of variance of models

A face-centred CCD with five centre points and an α value of 1 was chosen to avoid experiments lying outside the useful parametric region of interest (e.g., layer heights below machine capability, layer cure times shorter than the critical energy for gelation). The factors chosen in the experimental design matrix included the most commonly used parameters in mSLA printing, and were therefore deemed important for optimisation [4, 36-38]. It is worth noting that previous statistical approaches to mSLA optimisation have not included post-curing as a factor, despite being well known as an important factor [39]. Furthermore, while print orientation has been established as a factor that can influence the mechanical behaviour of the printed article in layer-by-layer AM, only two orientations were chosen (0° and 90° relative to build direction), and thus other orientations were not included as factors. One of the reasons for this was that, at intermediate orientations, support structures are needed, which could introduce surface defects during removal and thus affect the mechanical properties. However, the mechanical responses of both printing orientations were included thus allowing for the anisotropy ratio to be included as a response for optimisation.

The ANOVA is an important analysis tool to ensure the validity of a model. Given that the quadratic process order models for direct responses demonstrated adequate R^2, adjusted R^2, and predicted R^2 values alongside acceptable adequate precision values, their use for numerical optimisation could be established. However, it was evident that the indirect response of the anisotropy ratio did not present such, and was therefore deemed inappropriate for use in numerical optimisations. Furthermore, coefficients with significance were only incorporated into the model equations to ensure their validity for numerical optimisation.

4.2. Response surface plots

Differences in significant interactions could be observed between the horizontal and the vertical printing directions for both the tensile modulus and the tensile strength. This may be explained by the dependence of the interlayer bonding playing a stronger role in the vertical direction, where stress is applied perpendicular to the layers, unlike the case in the horizontal direction, where stress is applied parallel to the layers. Furthermore, in the vertical printing direction, an increase in tensile modulus was observed for smaller layer heights alongside longer layer cure times, although a local maximum in both layer cure time and layer height was observed. Generally, the observed increase in modulus with decreasing layer height was in agreement with other studies for SLA 3D printing [8, 25, 26]. Similarly to the tensile properties, the flexural properties demonstrated a comparable relationship to printing orientation. Again, given that the interlayer boundaries were perpendicular to the applied stress for vertically printed specimens, this suggested that the polymerisation both during 3D printing and during post-curing displayedan effect on the flexural modulus and flexural strength [6, 40, 41]. A previous study concluded that smaller layer heights and increasing overall UV exposure time (cumulative layer cure time and post-cure time) resulted in greater flexural strength, although very short exposure times (10-60 s) were used, and no statistical analysis was performed to identify significance between the parameters [42]. Nevertheless, the higher flexural strength

for smaller layer heights was in agreement with a previous study [43]. This observation may be because of a low degree of crosslinking throughout the layer for thicker layer heights, particularly when short layer cure times were used, and the effect was most appreciable on the response surface at short post-curing times.

Generally, modulus and strength related properties present a competing effect with ductility, such that greater modulus and strength is associated with a decrease in ductility owing to the degree of crosslinking within the polymer. Indeed, this was generally evident, such that an overall increase in post-curing that led to a higher degree of crosslinking resulted in a decrease in the strain at break for both tensile and flexural properties. However, for the tensile strain, a local minimum was observed, which may be the result of progressive crosslinking at layer interfaces, and which has been observed previously [44].

4.3. Numerical optimisation and relationship to Jacobs working curve

A numerical optimisation was performed to establish the printing parameters for desirable mechanical properties, resulting in a layer height of 50 µm, a layer cure time of 3.82 s, and a post-curing time of 13.5 min. First, the predicted optimised parameters were experimentally validated, resulting in experimental responses that generally matched the predicted mechanical properties with a low associated error. Generally, the low discrepancies between the predicted and the experimental responses validated the integrity of the models and thus provided a reliable platform for further optimisations. Although models with poor predictive capability (i.e., anisotropy ratios and Charpy) were not used in the optimisation, their predicted properties were retained to establish their efficacy. Interestingly, only the flexural strain anisotropy ratio and Charpy models failed to predict responses adequately, with a large error between the predicted and experimental responses, which was unsurprising considering that they had negative predicted R^2 values. Furthermore, the tensile and flexural strain in the vertical printing direction presented relatively poor predicted responses (error >5%) compared with the experimental values. Nevertheless, it was apparent that a smaller layer height was favoured for optimised mechanical properties, while an intermediate post-curing time provided balanced mechanical properties.

It was then of interest to compare the obtained optimised mechanical properties of the 3D printed specimens with those of the bulk polymer specimens. The 3D printed specimens generally displayed properties relatively close to those of the bulk polymer specimens, with exceptions for the tensile strain in the horizontal printing direction and the flexural strain in the vertical printing direction. The predominantly small differences in mechanical properties suggested that the optimised 3D printing parameters successfully minimised processing issues such as interlayer effects, which was further supported by the low anisotropy ratios observed in the 3D printed specimens. On the other hand, the relatively lower strains that were observed for the 3D printed specimens indicated that some deleterious processing issues were still apparent.

Having obtained satisfactory optimised 3D printing parameters with validated mechanical responses, it was of interest to ascertain whether there was a relationship to polymerisation effects using a Jacobs working curve. While the Jacobs working curve provided an estimate of the minimum UV exposure dose for gelation, it is well known that (meth)acrylates achieve gelation at partial overall conversions, thus resulting in a solid material without complete crosslinking. Furthermore, because of the attenuation of UV through the polymer, a differential degree of monomer conversion is established through the layer, with a higher degree of conversion closest to the incident radiation – that is, at the bottom of the layer [16, 43, 45-48]. On the other hand, exceeding the layer cure time for a specific layer height opens the potential for interlayer polymerisation during 3D printing, although it also implies a greater degree of crosslinking at the bottom of the layer, thus resulting in a reduced number of functional groups for the sequential layer to polymerise with [49, 50]. Conversely, with shorter layer cure times, interlayer polymerisation can be achieved through post-curing. However, it was found that the former scenario was favoured for optimised mechanical properties, such that optimised layer cure times that were appreciably higher than those of the Jacobs working curve were established. Furthermore, a nearly equal difference between the optimised layer cure times and those obtained from the Jacobs working curve was obtained. Although the linear least-squares fit of optimised layer cure times displayed a steeper gradient than that of the Jacobs working curve, it was apparent that a relatively consistent layer cure time beyond that obtained from the Jacobs working curve provided optimised mechanical property responses. This result suggested that achieving a degree of crosslinking between layers during additive manufacturing was favoured, compared with crosslinking during post-curing, which would be predominant when lower layer cure times were used [50].

5. CONCLUSION

The first example of using CCD and RSM analysis for multi-objective optimisation of mechanical properties for mSLA 3D printing was successfully demonstrated. The response surfaces that were produced could be used for numerical optimisation to predict adequately the 3D printing parameters for optimised mechanical properties. However, the predictive capabilities of the response surfaces for anisotropy ratios and Charpy impact properties were not adequate for optimisation. Nevertheless, the optimised printing parameters were experimentally validated and resulted in polymer specimens with mechanical properties close to those of bulk polymer specimens, indicating that processing influences such as interlayer effects could be minimised. Last, it was established that layer cure times greater than those obtained from a Jacobs working curve were established for optimised mechanical properties, implying that interlayer crosslinking during 3D printing was favoured.

REFERENCES

[1] J. J. Tully, and G. N. Meloni, "A scientist's guide to buying a 3D printer: How to choose the right printer for your laboratory," *Anal. Chem.,* 92(22), 14853-14860, 2020.

[2] T. Singh, S. Kumar, and S. Sehgal, "3D printing of engineering materials: A state of the art review," *Mater. Today Proc.,* 28**,** 1927-1931, 2020.

[3] A. Jandyal, I. Chaturvedi, I. Wazir, A. Raina, and M. I. Ul Haq, "3D printing – A review of processes, materials and applications in Industry 4.0," *Sustain. Oper. Comput.,* 3**,** 33-42, 2022.

[4] S. Junk, and F. Bär, "Design guidelines for additive manufacturing using masked stereolithography mSLA," *Procedia CIRP,* 119**,** 1122-1127, 2023.

[5] M. M. Gad, and S. M. Fouda, "Factors affecting flexural strength of 3D-printed resins: A systematic review," *J. Prosthodont.,* 32(S1), 96-110, 2023.

[6] D. L. Naik, and R. Kiran, "On anisotropy, strain rate and size effects in vat photopolymerization based specimens," *Addit. Manuf.,* 23**,** 181-196, 2018.

[7] F. de C. Magalhães, W. de O. Leite, and J. C. Campos Rubio, "A study of mechanical properties of photosensitive resins used in vat photopolymerization process," *J. Elastomers Plast.,* 56(6), 807-829, 00952443241256632, 2024.

[8] N. D. Borra, and V. S. N. Neigapula, "Parametric optimization for dimensional correctness of 3D printed part using masked stereolithography: Taguchi method," *Rapid Prototyp. J.,* 29**,** 1, 166-184, 2023.

[9] T. R. Mhmood, and N. K. AL-Karkhi, "Multiobjective optimization of stereolithography for dental bridge based on a simple shape model using Taguchi and response surface methods," *Appl. Sci.,* 13**(** 19), 10911, 2023.

[10] H. Sharifi, A. Adib, Z. Ahmadi, E. Gemikonakli, and M. Shahedi Asl, "Taguchi optimization of mask stereolithographic 3D printing parameters for tensile strengthening of functionally graded resins," *Int. J. Interact. Des. Manuf.,* 18(7), 4899-4910, 2024.

[11] B. Dhanunjayaro, and N. Naidu, "Parameter optimization for dimensional accuracy of vat photopolymerization 3D printed part: Taguchi approach," *AIP Conf. Proc.,* 3006(1), 040004, 2023.

[12] E. A. Garcia, C. Ayranci, and A. J. Qureshi, "Material property-manufacturing process optimization for form 2 vat-photo polymerization 3D printers," *J. Manuf. Mater. Process.,* 4(1), 12, 2020.

[13] D. Putra, M. Yanis, D. Seprianto, N. Amrillah, and H. Basri, "Optimization of production process parameters of DLP type 3D printer design for product roughness value," *Proceedings of the 4th Forum in Research, Science, and Technology*, 2589-4943, 2021.

[14] K. Chockalingam, N. Jawahar, K. Ramanathan, and P. Banerjee, "Optimization of stereolithography process parameters for part strength using design of experiments," *Int. J. Adv. Manuf. Tech.,* 29**,** 79-88, 2006.

[15] J. D. Kechagias, and N. Vidakis, "Parametric optimization of material extrusion 3D printing process: An assessment of Box-Behnken vs full-factorial experimental approach," *J. Adv. Manuf. Technol.,* 121(5), 3163-3172, 2022.

[16] Y. Yang, L. Li, and J. Zhao, "Mechanical property modeling of photosensitive liquid resin in stereolithography additive manufacturing: Bridging degree of cure with tensile strength and hardness," *Mater. Des.,* 162**,** 418-428, 2019.

[17] M. Forstmeier, J. LeBlanc, E. Warner, and K. Merlo, "Quantification of the effects of print parameters on the mechanical performance of low force stereolithography parts," *Int. J. Lightweight Mater. Manuf.,* 7(6), 958-967, 2024.

[18] E. Wang *et al.*, "Investigation and optimization of the impact of printing orientation on mechanical properties of resin sample in the low-force stereolithography additive manufacturing," *Mater.*, 15(19), 6743, 2022.
[19] R. B. S. Gowda, C. S. Udayagiri, and D. D. Narendra, "Studies on the process parameters of rapid prototyping technique (stereolithography) for the betterment of part quality," *Int. J. Manuf. Eng.*, 2014(1), 804705, 2014.
[20] M. Kazemi, and A. Rahimi, "Stereolithography process optimization for tensile strength improvement of products," *Rapid Prototyp. J.*, 24(4), 688-697, 2018.
[21] B. S. Raju, U. Chandrashekar, and D. N. Drakshayani, "Optimization studies on improving the strength characteristic for parts made of photosensitive polymer," *J. Inst. Eng. India Ser. D.*, 94(1), 35-41, 2013.
[22] S. Singh, A. Jain, P. Chaudhary, R. Gupta, and H. S. Mali, "Optimization of dimensional accuracy and surface roughness in m-SLA using response surface methodology," *Rapid Prototyp. J.*, 29(6), 1324-1339, 2023.
[23] M. Albaşkara, and S. Türkyilmaz, "Optimization of accuracy and surface roughness of 3D SLA printed materials with response surface method," *Int. J. 3D Printing Tech. Dig. Ind.*, 7(3), 403-414, 2024.
[24] A. Temiz, "The effects of process parameters on tensile characteristics and printing time for masked stereolithography components, analyzed using the response surface method," *J. Mater. Eng. Perform.*, 33, 9356-9365, 2024.
[25] A. Temiz, "The effect of build orientation on the mechanical properties of a variety of polymer AM-created triply periodic minimal surface structures," *J. Braz. Soc. Mech. Sci. Eng.*, 46(3), 121, 2024.
[26] M. Gregor, P. Grznar, S. Mozol, and L. Mozolova, "Design of simulation experiments using central composite design," *Acta Simulatio*, 9(2), 21-25, 2023.
[27] Z. Zhang, and B. Xiaofeng, "Comparison about the three central composite designs with simulation," *Proceedings of the 2009 International Conference on Advanced Computer Control*, 163-167, 2009.
[28] H. Vardhan Rai, Y. Kumar Modi, and A. Pare, "Process parameter optimization for tensile strength of 3D printed parts using response surface methodology," *Proceedings of the IOP Conference Series: Materials Science and Engineering*, 377, 012027, 2018.
[29] P. F. Jacobs, "Rapid prototyping & manufacturing: Fundamentals of stereolithography," *Soc. Manufact. Eng.*, 1992.
[30] *Standard test method for tensile properties of plastics*, ASTM D638-22, ASTM-International, West Conshohocken, PA, USA, 2022.
[31] *Standard test methods for flexural properties of unreinforced and reinforced plastics and electrical insulating materials*, ASTM D790-17, ASTM-International, West Conshohocken, PA, USA, 2017.
[32] *Standard test method for determining the charpy impact resistance of notched specimens of plastics*, ASTM D6110-18, ASTM-International, West Conshohocken, PA, USA, 2018.
[33] M. Štaffová, F. Ondreáš, J. Svatík, M. Zbončák, J. Jančář, and P. Lepcio, "3D printing and post-curing optimization of photopolymerized structures: Basic concepts and effective tools for improved thermomechanical properties," *Polym. Test.*, 108, 107499, 2022.
[34] T. J. Kolibaba *et al.*, "Results of an interlaboratory study on the working curve in vat photopolymerization," *Addit. Manuf.*, 84, 104082, 2024.
[35] Y. Wang, Y. Wang, C. Mao, and D. Mei, "Printing depth modeling, printing process quantification and quick-decision of printing parameters in micro-vat polymerization," *Mater. Des.*, 227, 111698, 2023.
[36] L. Schittecatte, V. Geertsen, D. Bonamy, T. Nguyen, and P. Guenoun, "From resin formulation and process parameters to the final mechanical properties of 3D printed acrylate materials," *MRS Commun.*, 13(3), 357-377, 2023.
[37] W. Piedra-Cascón, V. R. Krishnamurthy, W. Att, and M. Revilla-León, "3D printing parameters, supporting structures, slicing, and post-processing procedures of vat-polymerization additive manufacturing technologies: A narrative review," *J. Dent.*, 109, 103630, 2021.
[38] M. M. Prabhakar, A. Saravanan, A. H. Lenin, I. J. Ieno, K. Mayandi, and P. S. Ramalingam, "A short review on 3D printing methods, process parameters and materials," *Mater. Today Proc.*, 45, 6108-6114, 2021.
[39] B. Nowacki, P. Kowol, M. Kozioł, P. Olesik, J. Wieczorek, and K. Wacławiak, "Effect of post-process curing and washing time on mechanical properties of mSLA printouts," *Mater.*, 14(17), 4856, 2021.
[40] J. Stögerer, S. Baumgartner, T. Rath, and J. Stampfl, "Analysis of the mechanical anisotropy of stereolithographic 3D printed polymer composites," *Eur. J. Mater.*, 2(1), 12-32, 2022.
[41] D. Ambrosio, X. Gabrion, P. Malécot, F. Amiot, and S. Thibaud, "Influence of manufacturing parameters on the mechanical properties of projection stereolithography-manufactured specimens," *Int. J. Adv. Manuf. Tech.*, 106(1), 265-277, 2020.

[42] A. Milovanović *et al.*, "Compressive and flexural mechanical responses of components obtained through mSLA vat photopolymerization technology," *Theor. Appl. Fract. Mech.*, 131, 104406, 2024.
[43] L. Perea-Lowery, M. Gibreel, P. K. Vallittu, and L. Lassila, "Evaluation of the mechanical properties and degree of conversion of 3D printed splint material," *J. Mech. Behav. Biomed. Mater.*, 115, 104254, 2021.
[44] A. Pilipovic, L. Vukonic, "Optimization of post curing in mask stereolithography," *Cukurova Uni. J. Nat. Appl. Sci.*, 1(1), 31-40, 2022.
[45] H. Gojzewski *et al.*, "Layer-by-layer printing of photopolymers in 3D: How weak is the interface?" *ACS Appl. Mater. Interfaces*, 12(7), 8908-8914, 2020.
[46] R. Brighenti, M. P. Cosma, and S. Monchetti, "Mechanics of polymers obtained by layered photopolymerization," *Eur. J. Mech. A/Solids*, 106, 105323, 2024.
[47] C. I. Higgins, T. E. Brown, and J. P. Killgore, "Digital light processing in a hybrid atomic force microscope: *In situ*, nanoscale characterization of the printing process," *Addit. Manuf.*, 38, 101744, 2021.
[48] K. W. Ahmad, Z. Mohamad, N. Othman, S. H. C. Man, and M. Jusoh, "The mechanical properties of photopolymer prepared via 3D stereolithography printing: The effect of UV curing time and anisotropy," *Chem. Eng. Trans.*, 78, 2020.
[49] J. Lee *et al.*, "Average-accumulated normalized dose (A-AND) predicts ultimate tensile strength and elastic modulus of photopolymer printed by vat photopolymerization," *Addit. Manuf.*, 55, 102799, 2022.
[50] S. Park, A. M. Smallwood, and C. Y. Ryu, "Mechanical and thermal properties of 3D-printed thermosets by stereolithography," *J. Photopolym. Sci. Technol.*, 32(2), 227-232, 2019.